REPORT DOCUMENTATION PAGE

Form Approved
OMB NO. 0704-0188

1. AGENCY USE ONLY (Leave Blank)	2. REPORT DATE	3. REPORT TYPE AND DATES COVERED
	Oct. 2009	Reprint

4. TITLE AND SUBTITLE
The Effects of Spatial Diversity and Imperfect Channel Estimation on Wideband MC-DS-CDMA and MC-CDMA

5. FUNDING NUMBERS
W911NF0410224 (46637CIMUR)

6. AUTHOR(S)
A. S. Ling and L. B. Milstein

7. PERFORMING ORGANIZATION NAME(S) AND ADDRESS(ES)
University of California San Diego
9500 Gilman Drive, La Jolla, CA 92093-0407

8. PERFORMING ORGANIZATION REPORT NUMBER
N/A

9. SPONSORING / MONITORING AGENCY NAME(S) AND ADDRESS(ES)
U. S. Army Research Office
P.O. Box 12211
Research Triangle Park, NC 27709-2211

10. SPONSORING / MONITORING AGENCY REPORT NUMBER
N/A

11. SUPPLEMENTARY NOTES
The views, opinions and/or findings contained in this report are those of the author(s) and should not be construed as an official Department of the Army position, policy or decision, unless so designated by other documentation.

12 a. DISTRIBUTION / AVAILABILITY STATEMENT
Approved for public release; distribution unlimited.

12 b. DISTRIBUTION CODE
N/A

13. ABSTRACT (Maximum 200 words)

Abstract—In our previous work, we compared the theoretical bit error rates of multi-carrier direct sequence code division multiple access (MC-DS-CDMA) and multi-carrier code division multiple access (MC-CDMA). To ensure a fair comparison, we constrained both schemes to the same bandwidth, information rate, and energy-per-bit, and these constraints resulted in a possible trade-off between diversity gain and channel estimation errors between the two schemes. While only a single-input singleoutput (SISO) system was considered in our previous work, in this paper, we extend the comparison to a multiple-input multiple-output (MIMO) system which employs Alamouti spacetime block coding at each sub-carrier frequency to achieve spatial diversity. We consider only those cases where MC-CDMA has higher frequency diversity than MC-DS-CDMA. Since increases in diversity yield diminishing gains, we conclude that the addition of spatial diversity to this multi-carrier comparison benefits MCDS-CDMA more than MC-CDMA. To determine whether these gains for MC-DS-CDMA are enough to offset the difference in frequency diversity between the two schemes, we derive closed form expressions for the bit error probabilities of both schemes, and we compare the MIMO results against those of the SISO system for different information rates, number of users, and number of pilot symbols per channel estimate.

14. SUBJECT TERMS
MC-DS-CDMA, MC-CDMA, Alamouti spacetime block coding, frequency-selective Rayleigh fading, Hermitian quadratic form.

15. NUMBER OF PAGES
13

16. PRICE CODE
N/A

17. SECURITY CLASSIFICATION OR REPORT	18. SECURITY CLASSIFICATION ON THIS PAGE	19. SECURITY CLASSIFICATION OF ABSTRACT	20. LIMITATION OF ABSTRACT
UNCLASSIFIED	**UNCLASSIFIED**	**UNCLASSIFIED**	**UL**

NSN 7540-01-280-5500

Standard Form 298 (Rev.2-89)
Prescribed by ANSI Std. 239-18
298-102

Enclosure 1

The Effects of Spatial Diversity and Imperfect Channel Estimation on Wideband MC-DS-CDMA and MC-CDMA

Andrew S. Ling, *Member, IEEE,* and Laurence B. Milstein, *Fellow, IEEE*

***Abstract*—In our previous work, we compared the theoretical bit error rates of multi-carrier direct sequence code division multiple access (MC-DS-CDMA) and multi-carrier code division multiple access (MC-CDMA). To ensure a fair comparison, we constrained both schemes to the same bandwidth, information rate, and energy-per-bit, and these constraints resulted in a possible trade-off between diversity gain and channel estimation errors between the two schemes. While only a single-input single-output (SISO) system was considered in our previous work, in this paper, we extend the comparison to a multiple-input multiple-output (MIMO) system which employs Alamouti space-time block coding at each sub-carrier frequency to achieve spatial diversity. We consider only those cases where MC-CDMA has higher frequency diversity than MC-DS-CDMA. Since increases in diversity yield diminishing gains, we conclude that the addition of spatial diversity to this multi-carrier comparison benefits MC-DS-CDMA more than MC-CDMA. To determine whether these gains for MC-DS-CDMA are enough to offset the difference in frequency diversity between the two schemes, we derive closed-form expressions for the bit error probabilities of both schemes, and we compare the MIMO results against those of the SISO system for different information rates, number of users, and number of pilot symbols per channel estimate.**

***Index Terms*—MC-DS-CDMA, MC-CDMA, Alamouti space-time block coding, frequency-selective Rayleigh fading, Hermitian quadratic form.**

I. Introduction

MULTI-CARRIER signaling has been an active area of research over the past fifteen years. Two multi-carrier schemes which have been widely studied are multi-carrier direct sequence code division multiple access (MC-DS-CDMA) [1]–[7] and multi-carrier code division multiple access (MC-CDMA) [8]–[12]. When viewed in the frequency domain, these two schemes differ in the widths of their sub-bands: MC-DS-CDMA uses direct sequence spreading at each sub-carrier, while each sub-carrier in MC-CDMA is unspread. As a result, over a given bandwidth, MC-CDMA employs a larger number of sub-carriers than MC-DS-CDMA. On the one hand, this implies that MC-CDMA potentially has higher frequency diversity than MC-DS-CDMA when both schemes transmit at the same information rate; on the other hand, this also implies that the energy per sub-carrier is lower in MC-CDMA than in MC-DS-CDMA when both schemes use the same energy-per-bit. Since each MC-CDMA sub-carrier operates at a lower signal-to-noise ratio (SNR), the receiver's estimate of the channel gain at each sub-carrier frequency in MC-CDMA is more prone to error. Thus, there exists a possible trade-off between diversity gain and channel estimation errors between these two schemes. There are many papers which examine this trade-off, as well as other aspects, when comparing MC-DS-CDMA and MC-CDMA. To the best of our knowledge, however, the numerical results of these papers are all based on computer simulations [13]–[19].

In [20], we specifically considered the problem of whether a multi-carrier system should use spread or non-spread sub-carriers. Our approach to this problem involved a comparison of the theoretical bit error rates between MC-DS-CDMA and MC-CDMA and took into account the aforementioned trade-off between diversity gain and channel estimation errors. We were not concerned with optimizing performance or adhering to conventional implementations.[1] Rather, our main objective was to establish a fair comparison. Therefore, we required that both schemes use (1) the same bandwidth, information rate, and energy-per-bit; (2) the same combining scheme at the receiver (i.e., maximal ratio combining); and (3) the same pilot-based scheme to estimate the channel gains at each sub-carrier frequency.[2] We then derived closed-form expressions for the bit error probabilities of both schemes for two separate channel scenarios (i.e., two different cases for the coherence bandwidth of the channel), and we compared these error probabilities to determine the performance trade-offs that may result from using one scheme over the other.

In this paper, we extend our previous comparison between MC-DS-CDMA and MC-CDMA to a multiple-input multiple-

Paper approved by J. Wang, the Editor for Wireless Spread Spectrum of the IEEE Communications Society. Manuscript received April 12, 2008; revised September 17, 2008.

This work was supported by the US Army Research Office under MURI grant number W911NF-04-1-0224.

A. S. Ling was with the Department of Electrical and Computer Engineering, the University of California at San Diego, La Jolla, CA 92093 USA. He is now with the Space and Naval Warfare (SPAWAR) Systems Center Pacific, 53560 Hull Street, San Diego, CA 92152 USA (e-mail: andrewsling@gmail.com).

L. B. Milstein is with the Department of Electrical and Computer Engineering, the University of California at San Diego, La Jolla, CA 92093 USA (e-mail: milstein@ece.ucsd.edu).

Digital Object Identifier 10.1109/TCOMM.2009.10.080185

[1]Our MC-DS-CDMA system was based on the one proposed in [2] and studied further in [3]–[5]. Our MC-CDMA system was modeled after our MC-DS-CDMA system but still kept the main essence of MC-CDMA—namely, that the data at each MC-CDMA sub-carrier is unspread and that each sub-carrier is multiplied by a different chip in the spreading sequence.

[2]For both multi-carrier schemes, we assumed that the receiver has no knowledge of the coherence bandwidth of the channel and is forced to estimate the channel gains at each sub-carrier frequency.

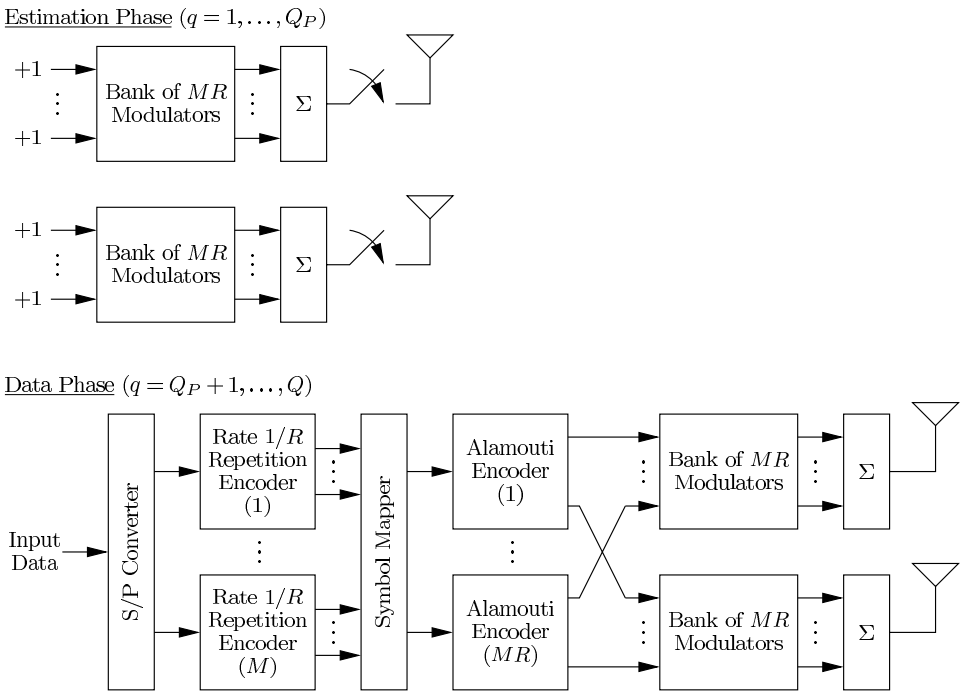

Fig. 1. Transmitter block diagram.

output (MIMO) system. For both multi-carrier schemes, we use Alamouti space-time block coding at each sub-carrier frequency to achieve spatial diversity in the absence of channel state information (CSI) at the transmitter [21]. By assuming (1) the coherence bandwidth of the channel is equal to the bandwidth of one MC-DS-CDMA sub-band, and (2) the number of data symbols transmitted in parallel, M, is such that $M > 1$, we consider only those cases where MC-CDMA has higher frequency diversity than MC-DS-CDMA, because these are the only instances in which there is a performance trade-off between the two schemes [20]. Since increases in diversity yield diminishing gains, we conclude that the addition of spatial diversity to this multi-carrier comparison benefits MC-DS-CDMA more than MC-CDMA. To determine whether these gains for MC-DS-CDMA are enough to offset the difference in frequency diversity between the two schemes, we use a quadratic-form-based technique to derive closed-form expressions for the bit error probabilities of both schemes, and we compare the numerical results of the MIMO system against those of the SISO system for different information rates, number of users, and number of pilot symbols per channel estimate.

This paper is organized as follows. In Section II, we present the system model assuming a general multi-carrier signaling scheme. We apply MC-CDMA and MC-DS-CDMA signaling to this system model in Section III, and we analyze their error probability performances in Section IV. The numerical results of the MIMO system are then compared against those of the SISO system in Section V, and Section VI concludes the paper.

Notation: Lowercase (uppercase) boldface letters denote column vectors (matrices); $\mathbf{I}_N$ and $\mathbf{0}_N$ are the $N \times N$ identity and zero matrices, respectively; $(\cdot)^T$, $(\cdot)^*$, and $(\cdot)^H$ denote transpose, complex conjugate, and complex conjugate transpose, respectively; $\otimes$ denotes the Kronecker product; $\delta_{n,m} \triangleq \delta[n-m]$, where $\delta[\cdot]$ is the Kronecker delta function.

II. General MIMO Multi-Carrier System Model

A. Overview

Consider an uplink scenario involving K asynchronous users. Assume two antennas at each transmitter and two antennas at the receiver. The available bandwidth is the same for each user and is divided into S bandlimited, non-overlapping frequency sub-bands of equal width.[3] We assume each sub-band is associated with a sub-carrier frequency and has a bandwidth of W.

In the time domain, the transmissions made at each sub-carrier are structured into frames, each consisting of Q time slots. As in [20], we assume a slowly-varying channel which remains constant over the duration of a frame, and we designate the first Q_P time slots of each frame as the *estimation phase* and the remaining $Q_D = Q - Q_P$ time slots as the *data phase*. During each time slot of the data phase, both antennas simultaneously transmit M distinct binary data symbols in parallel across the S sub-bands, where each symbol is repeated on R sub-carriers. Thus, we have $S = MR$, and the overall system bandwidth is equal to $SW = MRW$. Similarly, during the estimation phase, we transmit M pilot symbols ($+1$'s) in parallel, and we spread the energy of each pilot symbol across R sub-bands. However, pilot symbols are transmitted on the first antenna only during the odd time slots and on the second antenna only during the even time slots. As a result, only the odd (even) time slots are used to estimate the channel gains associated with the first (second) transmit antenna, and each estimate is formed from $Q_P/2$ pilot symbols.[4] To keep

[3]Spectral efficiency is not a concern in this comparison, so we do not insist on using minimum sub-carrier spacing and having the sub-bands overlap.

[4]We assume Q_P is even.

the total energy transmitted from the two antennas the same over all of the time slots, we also use a different transmit amplitude during the estimation phase. Our motivation for imposing this energy constraint, as well as for using the on-off pilot transmission scheme, is to maintain the same energy-per-pilot symbol between this system and the SISO system in [20]. By doing so, channel estimates formed from the same number of pilot symbols will be of the same quality in both the SISO and MIMO systems.

B. Transmitter

The transmitter block diagram is shown in Fig. 1. During the estimation phase, the on-off transmission of pilot symbols on all the sub-carriers is modeled using the switches at the two antennas. The switch for the first (second) antenna is closed during the odd (even) time slots and open during the even (odd) times slots. The details of the multi-carrier modulation blocks will be given in Section III when we consider MC-CDMA and MC-DS-CDMA.

During the data phase, the input data is modeled as an independent random binary sequence with bit rate $1/T$. The serial-to-parallel (S/P) converter produces M parallel sequences, and we label each group of M symbols as $\{a_{p,q,m}^{(k)}\}_{m=1}^{M}$, where p is the frame index, q is the time slot index, and k is the user index. A rate $1/R$ repetition code is applied to each of these M symbols, and the resulting MR symbols are mapped to the MR sub-carriers in such a way that maximizes the frequency separation between adjacent repetitions of a symbol. We denote the frequency to which the i-th repetition of the m-th symbol is mapped by $f_{m,i}$.[5] After symbol mapping, Alamouti space-time block coding is performed at each sub-carrier frequency, and the outputs of the encoders are fed through the two banks of modulators. Finally, the signals are combined and transmitted over the two antennas.

To represent the transmitted signals at each frequency during the estimation and data phases under a common mathematical framework, we define $b_{p,q,u,m}^{(k)}$ as the k-th user's input to the modulators at frequencies $\{f_{m,i}\}_{i=1,\ldots,R}$ of the u-th transmit antenna during the q-th time slot of the p-th frame. As shown in Table I, for $q = 1, \ldots, Q_P$, $b_{p,q,u,m}^{(k)}$ is equal to either $+1$ or 0, while for $q = Q_P+1, \ldots, Q$, $b_{p,q,u,m}^{(k)}$ is equal to the output of the Alamouti encoder. The transmitted signal for the k-th user is given by the 2×1 vector

$$\mathbf{s}^{(k)}(t) = \sum_{m=1}^{M} \sum_{i=1}^{R} \mathrm{Re}\left\{ \tilde{\mathbf{s}}_{m,i}^{(k)}(t) e^{j2\pi f_{m,i} t} \right\}, \qquad (1)$$

where $\tilde{\mathbf{s}}_{m,i}^{(k)}(t) = [\tilde{s}_{1,m,i}^{(k)}(t)\ \tilde{s}_{2,m,i}^{(k)}(t)]^T$ and the expression for $\tilde{s}_{u,m,i}^{(k)}(t)$ $(u = 1, 2)$ depends on the multi-carrier scheme used.

C. Channel

Assume the two antennas at both the transmitter and receiver are sufficiently spaced, such that the channels between different transmit-receive antenna pairs are independent. Each channel is frequency-selective with respect to the overall system bandwidth, but each sub-band is assumed to be frequency non-selective with Rayleigh-distributed fade amplitudes. Consequently, our use of Alamouti space-time block coding yields fourth-order spatial diversity at each sub-carrier frequency; the theoretical frequency diversity gain, however, depends on the correlation of the channel gains across the different sub-bands, which is a function of the coherence bandwidth of the channel.

In the absence of Doppler effects, there is no inter-channel interference between adjacent sub-bands since they do not overlap. Assuming perfect power control, the complex lowpass equivalent received signal at frequency $f_{m,i}$ is then given by the 2×1 vector $\tilde{\mathbf{r}}_{m,i}(t) = [\tilde{r}_{1,m,i}(t)\ \tilde{r}_{2,m,i}(t)]^T$, where

$$\tilde{r}_{v,m,i}(t) = \sum_{k=1}^{K} \sum_{u=1}^{2} g_{v,u,m,i}^{(k)} \tilde{s}_{u,m,i}^{(k)}(t-\tau^{(k)}) + \tilde{n}_v(t), \quad v = 1, 2. \qquad (2)$$

In the above equation, $g_{v,u,m,i}^{(k)} \triangleq \alpha_{v,u,m,i}^{(k)} e^{j\theta_{v,u,m,i}^{(k)}}$ is a zero-mean circularly symmetric complex Gaussian random variable representing the k-th user's channel gain at frequency $f_{m,i}$ between the u-th transmit antenna and the v-th receive antenna, where $\alpha_{v,u,m,i}^{(k)}$ is a Rayleigh random variable with unit second moment, and $\theta_{v,u,m,i}^{(k)}$ is a uniform random variable over $[0, 2\pi)$. The $\{g_{v,u,m,i}^{(k)}\}$ are identically distributed, but their joint statistics depend on the coherence bandwidth of the channel. Also, $\tau^{(k)}$ represents the relative time delay between the k-th user and the desired user, and $\tilde{n}_v(t)$ is a zero-mean complex additive white Gaussian noise (AWGN) random process with two-sided power spectral density N_0. The noise processes at the two receive antennas are assumed to be independent.

TABLE I
DEFINITION OF $b_{p,q,u,m}^{(k)}$

Estimation phase	$b_{p,q,u,m}^{(k)} = \begin{cases} \delta_{u,1}, & q \text{ odd} \\ \delta_{u,2}, & q \text{ even} \end{cases}$
Data phase	$b_{p,q,u,m}^{(k)} = \begin{cases} a_{p,q,m}^{(k)}, & u = 1,\ q \text{ odd} \\ a_{p,q+1,m}^{(k)}, & u = 2,\ q \text{ odd} \\ -a_{p,q,m}^{(k)}, & u = 1,\ q \text{ even} \\ a_{p,q-1,m}^{(k)}, & u = 2,\ q \text{ even} \end{cases}$

D. Receiver

The block diagram for the receiver is shown in Fig. 2. At each antenna, the received signal first passes through a bank of MR demodulators. We label the output of the demodulator at frequency $f_{m,i}$ of the v-th receive antenna during the estimation and data phases as $W_{q,v,m,i}$ $(q = 1, \ldots, Q_P)$ and $Y_{q,v,m,i}$ $(q = Q_P + 1, \ldots, Q)$, respectively. During the estimation phase, the estimate of $g_{v,u,m,i}^{(k)}$, $\hat{W}_{v,u,m,i}$, is formed by taking a sample average of the $\{W_{q,v,m,i}\}$ during the odd

[5]Hence, there exists a one-to-one correspondence between the pair (m, i) and the sub-carrier frequency $f_{m,i}$.

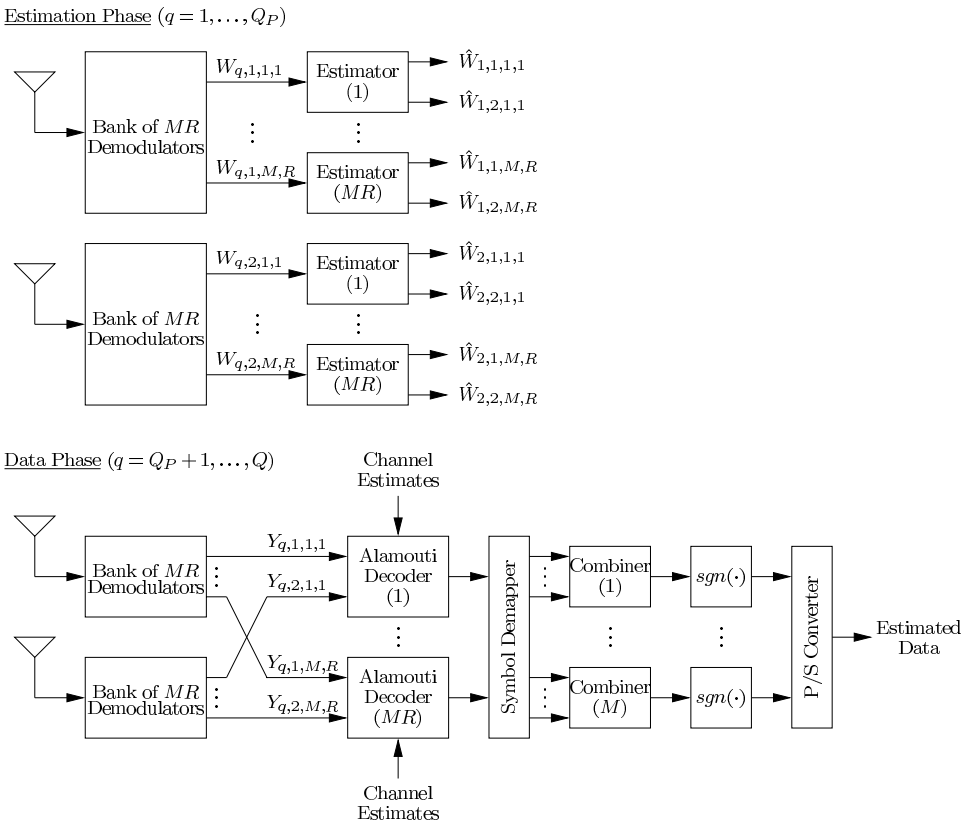

Fig. 2. Receiver block diagram.

or even time slots:

$$\hat{W}_{v,u,m,i} = \begin{cases} \dfrac{1}{A_0}\left(\dfrac{1}{Q_P/2}\displaystyle\sum_{\substack{q=1\\ q \text{ odd}}}^{Q_P} W_{q,v,m,i}\right), & u = 1, \\ \dfrac{1}{A_0}\left(\dfrac{1}{Q_P/2}\displaystyle\sum_{\substack{q=1\\ q \text{ even}}}^{Q_P} W_{q,v,m,i}\right), & u = 2, \end{cases} \tag{3}$$

where the normalizing constant A_0 ensures that $\hat{W}_{v,u,m,i}$ is an unbiased estimate of $g^{(k)}_{v,u,m,i}$. During the data phase, the $\{Y_{q,v,m,i}\}$ at each sub-carrier frequency over two consecutive time slots feed into a linear Alamouti decoder, which outputs the 2×1 vector

$$\mathbf{z}_{q,m,i} = \hat{\mathbf{G}}^H_{m,i}\mathbf{y}_{q,m,i} = [Z_{q,m,i}\ Z_{q+1,m,i}]^T, \tag{4}$$

where q is an odd integer in the range $Q_P + 1, \ldots, Q$. In the above equations, we have

$$\hat{\mathbf{G}}_{m,i} = \begin{bmatrix} \hat{W}_{1,1,m,i} & \hat{W}_{1,2,m,i} \\ \hat{W}_{2,1,m,i} & \hat{W}_{2,2,m,i} \\ \hat{W}^*_{1,2,m,i} & -\hat{W}^*_{1,1,m,i} \\ \hat{W}^*_{2,2,m,i} & -\hat{W}^*_{2,1,m,i} \end{bmatrix} \triangleq [\hat{\mathbf{w}}_{1,m,i}\ \hat{\mathbf{w}}_{2,m,i}], \tag{5}$$

$$\mathbf{y}_{q,m,i} = \begin{bmatrix} Y_{q,1,m,i} \\ Y_{q,2,m,i} \\ Y^*_{q+1,1,m,i} \\ Y^*_{q+1,2,m,i} \end{bmatrix}, \tag{6}$$

such that $Z_{q,m,i} = \hat{\mathbf{w}}^H_{1,m,i}\mathbf{y}_{q,m,i}$ and $Z_{q+1,m,i} = \hat{\mathbf{w}}^H_{2,m,i}\mathbf{y}_{q,m,i}$. We focus on the detection of $Z_{q,m,i}$. After Alamouti decoding, the demapper groups together the R variables associated with each of the M parallel data symbols and feeds them into a bank of M combiners. The output of the m-th combiner is expressed as

$$\begin{aligned} \hat{Z}_{q,m} &= \text{Re}\left\{\sum_{i=1}^{R} Z_{q,m,i}\right\} \\ &= \sum_{i=1}^{R}\left\{\frac{1}{2}\hat{\mathbf{w}}^H_{1,m,i}\mathbf{y}_{q,m,i} + \frac{1}{2}\mathbf{y}^H_{q,m,i}\hat{\mathbf{w}}_{1,m,i}\right\}, \end{aligned} \tag{7}$$

where, again, q is an odd integer in the range $Q_P + 1, \ldots, Q$, and the m-th data symbol during the q-th time slot is decoded as $\text{sgn}\left\{\hat{Z}_{q,m}\right\}$. Finally, parallel-to-serial (P/S) conversion gives the estimated data sequence.

E. Probability of Error

By defining

$$\mathbf{w}_m = \left[\tilde{\mathbf{w}}^T_{m,1} \quad \cdots \quad \tilde{\mathbf{w}}^T_{m,R}\right]^T, \tag{8}$$

$$\mathbf{y}_{q,m} = \left[\tilde{\mathbf{y}}^T_{q,m,1} \quad \cdots \quad \tilde{\mathbf{y}}^T_{q,m,R}\right]^T, \tag{9}$$

where

$$\tilde{\mathbf{w}}_{m,i} = \left[\hat{W}_{1,1,m,i} \quad \hat{W}_{2,1,m,i} \quad \hat{W}_{1,2,m,i} \quad \hat{W}_{2,2,m,i}\right]^T, \tag{10}$$

$$\tilde{\mathbf{y}}_{q,m,i} = \left[Y_{q,1,m,i} \quad Y_{q,2,m,i} \quad Y_{q+1,1,m,i} \quad Y_{q+1,2,m,i}\right]^T, \tag{11}$$

we can re-express $\hat{Z}_{q,m}$ in (7) as a Hermitian quadratic form in zero-mean complex Gaussian random variables,

$$\hat{Z}_{q,m} = \mathbf{v}^H_{q,m}\mathbf{F}\mathbf{v}_{q,m}, \tag{12}$$

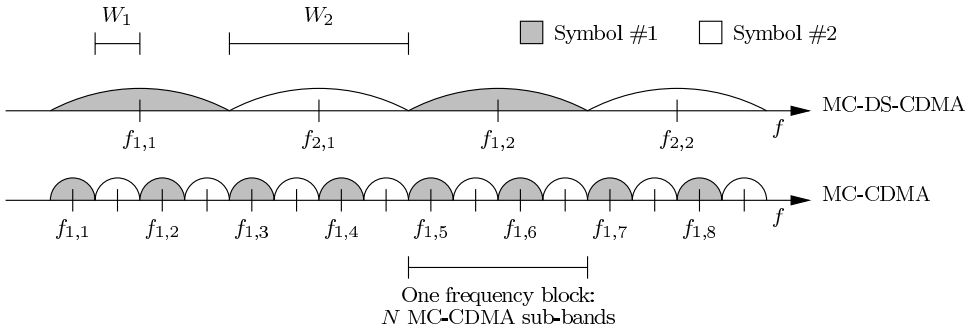

Fig. 3. Spectra of the MC-DS-CDMA and MC-CDMA signals. In this example, $M = 2$ parallel data symbols are each repeated across $R_1 = 8$ and $R_2 = 2$ sub-carriers in MC-CDMA and MC-DS-CDMA, respectively, where $N = 4$ is the processing gain in each MC-DS-CDMA sub-band. We assume the coherence bandwidth of the channel, $(\Delta f)_c$, is equal to W_2.

where

$$\mathbf{v}_{q,m} = \begin{bmatrix} \mathbf{w}_m \\ \mathbf{y}_{q,m} \end{bmatrix}, \quad \mathbf{F} = \frac{1}{2}\begin{bmatrix} \mathbf{0}_{4R} & \mathbf{I}_{4R} \\ \mathbf{I}_{4R} & \mathbf{0}_{4R} \end{bmatrix}. \tag{13}$$

Assuming a $+1$ was transmitted, the bit error probability is given by

$$P_e = P\left\{ \hat{Z}_{q,m} < 0 \,\middle|\, a^{(k)}_{p,q,m} = +1 \right\}. \tag{14}$$

A general method for obtaining a closed-form expression of (14) is outlined in Appendix A.

III. MC-CDMA vs. MC-DS-CDMA

A. Overview

We now apply MC-CDMA and MC-DS-CDMA signaling to the system model presented in Section II. To distinguish the system parameters between the two schemes, we write $S = S_1$, $W = W_1$, and $R = R_1$ for MC-CDMA and $S = S_2$, $W = W_2$, and $R = R_2$ for MC-DS-CDMA. Each MC-CDMA sub-band is non-spread and has a symbol rate of $1/T_s$, where $T_s = \frac{Q_D}{Q} MT$. Therefore, the bandwidth of each sub-band is $W_1 = 1/T_s$. On the other hand, each MC-DS-CDMA sub-band has a processing gain (spreading factor) of N, so $W_2 = NW_1 = 1/T_c$, where $1/T_c = N/T_s$ is the chip rate. Since the two multi-carrier schemes are constrained to the same information rate and bandwidth, we have $MR_1W_1 = MR_2W_2$, which implies $R_1 = NR_2$. An example of how the two schemes compare in the frequency domain is given in Fig. 3.

In the following comparison, we assume: (1) the channel is the same for both schemes, and the coherence bandwidth of the channel, $(\Delta f)_c$, is equal to W_2; (2) perfect carrier, chip, and symbol synchronization are established at the receiver; and (3) all K users use long spreading sequences, which are modeled as independent random binary sequences of ± 1's.

B. MC-CDMA

1) Transmitter: The block diagram of the MC-CDMA modulator at frequency $f_{m,i}$ of the u-th transmit antenna, as shown in Fig. 4, is identical to the one in [20]. Each symbol at the input of the MC-CDMA modulator is multiplied by only a single chip from the k-th user's spreading sequence, $C^{(k)}_{p,q,m,i}$. The resulting sequence modulates an impulse train and passes through a chip wave-shaping filter denoted by $H_1(f)$. Finally, the output signal of the filter modulates the corresponding sub-carrier.

The transmitted signal for the k-th user is given by (1), where

$$\tilde{s}^{(k)}_{u,m,i}(t) = \sum_{p=-\infty}^{\infty} \sum_{q=1}^{Q} A_{1,q}\, b^{(k)}_{p,q,u,m}\, C^{(k)}_{p,q,m,i} \cdot h_1\big[t - (pQ + q - 1)T_s\big]. \tag{15}$$

In the above equation, $h_1(t)$ is the impulse response of the chip wave-shaping filter $H_1(f)$, and $A_{1,q}$ is the transmit amplitude during the q-th time slot:

$$A_{1,q} = \begin{cases} A_{1e}, & q = 1, \ldots, Q_P, \\ A_{1d}, & q = Q_P + 1, \ldots, Q. \end{cases} \tag{16}$$

To keep the total energy transmitted from the two antennas the same over all time slots, we choose $A_{1d} = A_{1e}/\sqrt{2}$. As a result, the energy per bit can be shown to equal $E_{b1} = \frac{1}{2} R_1 A^2_{1e} = R_1 A^2_{1d}$ [22, Appendix P].

2) Channel: Given $(\Delta f)_c = W_2 = NW_1 \gg W_1$, the coherence bandwidth of the channel spans multiple MC-CDMA sub-bands, which means that the sub-bands may be highly correlated. We assume a *correlated block fading* model in which the MR_1 sub-bands are grouped into MR_1/N frequency blocks—each block of N sub-bands corresponds to one MC-DS-CDMA sub-band, and the number of repetitions-per-data symbol within a block is equal to $R_b \triangleq N/M$ (see Fig. 3). We assume flat fading across each block, such that the N fade amplitudes associated with each block are identical (i.e., perfectly correlated). Also, we assume the fade amplitudes associated with any two sub-bands from different blocks are independent. Thus, even though each symbol is transmitted across R_1 sub-carriers, the effective order of frequency diversity per data symbol is only MR_1/N, and the overall diversity gain per data symbol is $4MR_1/N$, where the factor of 4 comes from the spatial diversity. Note that the frequency diversity gain for MC-CDMA does not change when we vary M, since MR_1 and N are both fixed.

3) Receiver: The complex equivalent lowpass version of the MC-CDMA demodulator in [20] is shown in Fig. 4, where $\tilde{h}_{m,i,1}(t) = h^*_1(-t)$ is the complex equivalent lowpass impulse response of the bandpass filter. The despreading operation in MC-CDMA simply involves multiplication by a single chip.

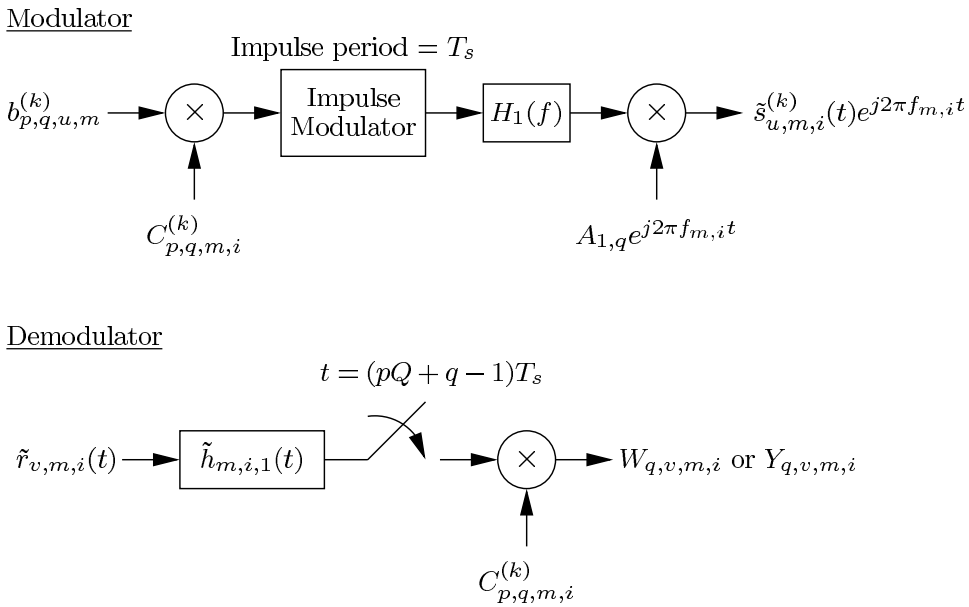

Fig. 4. MC-CDMA modulator at frequency $f_{m,i}$ of the u-th transmit antenna, and complex equivalent lowpass version of the MC-CDMA demodulator at frequency $f_{m,i}$ of the v-th receive antenna.

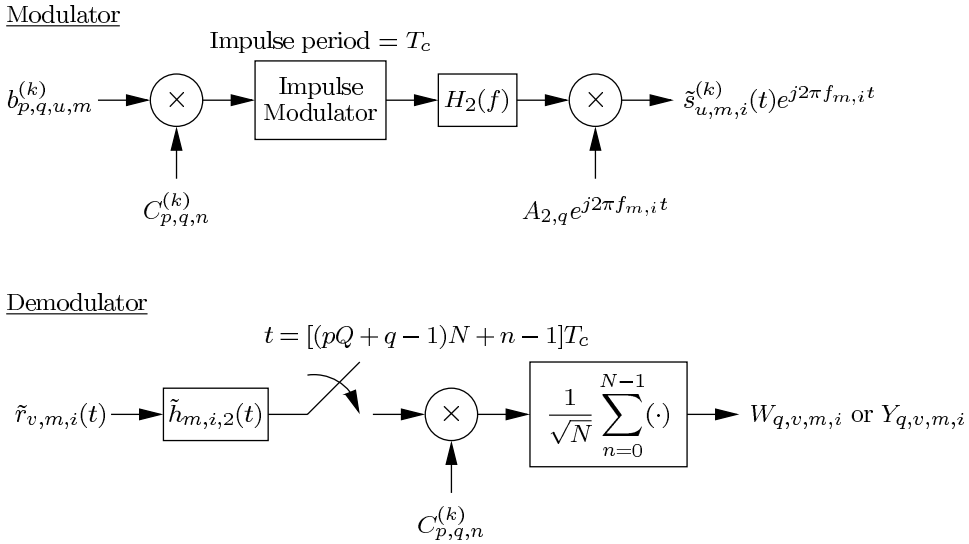

Fig. 5. MC-DS-CDMA modulator at frequency $f_{m,i}$ of the u-th transmit antenna, and complex equivalent lowpass version of the MC-DS-CDMA demodulator at frequency $f_{m,i}$ of the v-th receive antenna.

Assume $H_1(f)$ is of unit energy, i.e., $\int_{-\infty}^{\infty} |H_1(f)|^2\, df = 1$. We define $x_1(t) \Leftrightarrow X_1(f) \triangleq |H_1(f)|^2$ and assume

$$X_1(f) = \begin{cases} T_s, & -\frac{1}{2T_s} < f < \frac{1}{2T_s}, \\ 0, & \text{otherwise}, \end{cases} \Leftrightarrow x_1(t) = \frac{\sin \pi t/T_s}{\pi t/T_s}. \tag{17}$$

Since $X_1(f)$ satisfies the Nyquist criterion, inter-symbol interference is not present.

C. MC-DS-CDMA

1) Transmitter: The block diagram of the MC-DS-CDMA modulator at frequency $f_{m,i}$ of the u-th transmit antenna is identical to the one in [20] (see Fig. 5). During each time slot, $b^{(k)}_{p,q,u,m}$ is multiplied by N chips in the spreading sequence, $\{C^{(k)}_{p,q,n}\}_{n=1}^{N}$. The transmitted signal for the k-th user is also given by (1), but with

$$\tilde{s}^{(k)}_{u,m,i}(t) = \sum_{p=-\infty}^{\infty} \sum_{q=1}^{Q} \sum_{n=1}^{N} A_{2,q}\, b^{(k)}_{p,q,u,m}\, C^{(k)}_{p,q,n} \cdot h_2\big\{t - [(pQ + q - 1)N + n - 1]T_c\big\}, \tag{18}$$

where $h_2(t)$ is the impulse response of the chip wave-shaping filter $H_2(f)$, and $A_{2,q}$ is the transmit amplitude during the q-th time slot, which is defined as

$$A_{2,q} = \begin{cases} A_{2e}, & q = 1, \ldots, Q_P, \\ A_{2d}, & q = Q_P + 1, \ldots, Q. \end{cases} \tag{19}$$

We choose $A_{2d} = A_{2e}/\sqrt{2}$, such that the energy per bit is equal to $E_{b2} = \frac{1}{2} R_2 A_{2e}^2 N = R_2 A_{2d}^2 N$ [22, Appendix P].

2) Channel: With $(\Delta f)_c = W_2$, we assume flat fading in each MC-DS-CDMA sub-band and independent fading between different sub-bands. As a result, the order of frequency diversity seen by each data symbol is R_2, and the overall diversity gain per data symbol is $4R_2$. Since $R_1 = NR_2$, we have $4MR_1/N = 4MR_2 \geq 4R_2$, which implies that MC-CDMA has M times the diversity of MC-DS-CDMA.

3) Receiver: We use the complex equivalent lowpass version of the MC-DS-CDMA demodulator in [20], where $\tilde{h}_{m,i,2}(t) = h_2^*(-t)$ (see Fig. 5). In contrast to MC-CDMA, the despreading operation in MC-DS-CDMA involves multiplication by N chips. We define $x_2(t) \Leftrightarrow X_2(f) \stackrel{\Delta}{=} |H_2(f)|^2$, where the expression for $X_2(f)$ is given by replacing T_s with T_c in (17). Since $X_2(f)$ also satisfies the Nyquist criterion, inter-symbol interference is not present.

IV. Performance Analysis

In this section, we present the expressions for $W_{q,v,m,i}$, $Y_{q,v,m,i}$, and $\hat{W}_{v,u,m,i}$ as they apply to MC-CDMA and MC-DS-CDMA. We also give closed-form results for the bit error probabilities of both schemes, assuming the desired user is $k = 1$ (hence, $\tau^{(1)} = 0$).

A. MC-CDMA

1) Demodulator Output: The output of the demodulator at frequency $f_{m,i}$ of the v-th antenna during the q-th time slot is given by

$$W_{q,v,m,i} = A_{1e}\, g^{(1)}_{v,u,m,i} + I_{W_{q,v,m,i}} + N_{W_{q,v,m,i}}, \quad q = 1, \ldots, Q_P, \tag{20}$$

$$Y_{q,v,m,i} = A_{1d} \sum_{u=1}^{2} b^{(1)}_{p,q,u,m}\, g^{(1)}_{v,u,m,i} + I_{Y_{q,v,m,i}} + N_{Y_{q,v,m,i}}, \quad q = Q_P + 1, \ldots, Q, \tag{21}$$

where

$$I_{W_{q,v,m,i}} = C^{(1)}_{p,q,m,i} \sum_{k=2}^{K} \sum_{u=1}^{2} g^{(k)}_{v,u,m,i} \cdot \sum_{p'=-\infty}^{\infty} \sum_{q'=1}^{Q} A_{1,q'} b^{(k)}_{p',q',u,m} C^{(k)}_{p',q',m,i} \cdot x_1[t - (p'Q + q' - 1)T_s - \tau^{(k)}]\Big|_{t=(pQ+q-1)T_s} \tag{22}$$

and

$$N_{W_{q,v,m,i}} = C^{(1)}_{p,q,m,i} \left(\tilde{n}_v(t) * \tilde{h}_{m,i,1}(t)\right)\Big|_{t=(pQ+q-1)T_s} \tag{23}$$

represent the multiple access interference (MAI) due to the other $K-1$ users and the contribution of the AWGN to the test statistic, respectively. The expressions for $I_{Y_{q,v,m,i}}$ and $N_{Y_{q,v,m,i}}$ are identical to (22) and (23), respectively, except they are associated with a different range of values for q. Note that the desired signal and AWGN terms are both zero-mean complex Gaussian. Thus, in the single-user case, $W_{q,v,m,i}$ and $Y_{q,v,m,i}$ are both zero-mean complex Gaussian random variables. When K is large, the MAI terms are approximated as zero-mean complex Gaussian random variables, and $W_{q,v,m,i}$ and $Y_{q,v,m,i}$ are approximated as zero-mean complex Gaussian random variables as well.

2) Channel Estimation: Substituting (20) into (3) and setting $A_0 = A_{1e}$, the estimate of $g^{(1)}_{v,u,m,i}$ is given by

$$\hat{W}_{v,u,m,i} = \begin{cases} g^{(1)}_{v,u,m,i} + \dfrac{1}{A_{1e}} \dfrac{1}{Q_P/2} \displaystyle\sum_{\substack{q=1 \\ q \text{ odd}}}^{Q_P} \Upsilon_{W_{q,v,m,i}}, & u = 1, \\ g^{(1)}_{v,u,m,i} + \dfrac{1}{A_{1e}} \dfrac{1}{Q_P/2} \displaystyle\sum_{\substack{q=1 \\ q \text{ even}}}^{Q_P} \Upsilon_{W_{q,v,m,i}}, & u = 2, \end{cases} \tag{24}$$

where $\Upsilon_{W_{q,v,m,i}} \stackrel{\Delta}{=} I_{W_{q,v,m,i}} + N_{W_{q,v,m,i}}$. Since $\hat{W}_{v,u,m,i}$ is a linear combination of the $\{W_{q,v,m,i}\}$, it is also a zero-mean complex Gaussian random variable when $K = 1$ and is approximated as a zero-mean complex Gaussian random variable when K is large.

From estimation theory, both $\{W_{q,v,m,i}\}_{q \text{ odd}}$ and $\{W_{q,v,m,i}\}_{q \text{ even}}$ represent *linear models*. The classical approach assumes $g^{(k)}_{v,u,m,i}$ is deterministic, and we can show that $\hat{W}_{v,u,m,i}$ is the minimum variance unbiased (MVU) estimator [23]. On the other hand, the Bayesian approach assumes $g^{(1)}_{v,u,m,i}$ is zero-mean complex Gaussian. It can be shown that the minimum mean square error (MMSE) estimate of $g^{(1)}_{v,u,m,i}$ is just a scaled version of $\hat{W}_{v,u,m,i}$, and that both the MVU and MMSE estimators yield the same probability of error [22, Appendix F].

3) Probability of Error: Using the approach outlined in Appendix A, the probability of error is derived as (see Appendix B)

$$\begin{aligned} P_e = {} & \left(\frac{1}{2}\right)^b \sum_{i_2=0}^{b-1} \binom{b-1+i_2}{i_2} \left(\frac{1}{2}\right)^{i_2} \\ & \cdot \left(\frac{1-\mu_{31}}{2}\right)^a \sum_{i_3=0}^{b-1-i_2} \binom{a-1+i_3}{i_3} \left(\frac{1+\mu_{31}}{2}\right)^{i_3} \\ & \cdot \left(\frac{1-\mu_{41}}{2}\right)^a \sum_{r=0}^{b-1-i_2-i_3} \binom{a-1+r}{r} \left(\frac{1+\mu_{41}}{2}\right)^r \\ & + \left(\frac{1-\mu_{13}}{2}\right)^b \sum_{i_1=0}^{a-1} \binom{b-1+i_1}{i_1} \left(\frac{1+\mu_{13}}{2}\right)^{i_1} \\ & \cdot \left(\frac{1-\mu_{23}}{2}\right)^b \sum_{i_2=0}^{a-1-i_1} \binom{b-1+i_2}{i_2} \left(\frac{1+\mu_{23}}{2}\right)^{i_2} \\ & \cdot \left(\frac{1-\mu_{43}}{2}\right)^a \sum_{r=0}^{a-1-i_1-i_2} \binom{a-1+r}{r} \\ & \cdot \left(\frac{1+\mu_{43}}{2}\right)^r, \end{aligned} \tag{25}$$

where $a = 4MR_1/N$, $b = 4(R_1 - MR_1/N)$,

$$\mu_{31} = \frac{R_b - \sqrt{d\left(\frac{E_{b1}}{N_0}\right)} - \sqrt{2}\frac{1}{\sqrt{Q_P/2}} c_1\left(\frac{E_{b1}}{N_0}\right)}{R_b - \sqrt{d\left(\frac{E_{b1}}{N_0}\right)} + \sqrt{2}\frac{1}{\sqrt{Q_P/2}} c_1\left(\frac{E_{b1}}{N_0}\right)}, \tag{26}$$

$$\mu_{41} = \frac{R_b + \sqrt{d\left(\frac{E_{b1}}{N_0}\right)} - \sqrt{2}\frac{1}{\sqrt{Q_P/2}}c_1\left(\frac{E_{b1}}{N_0}\right)}{R_b + \sqrt{d\left(\frac{E_{b1}}{N_0}\right)} + \sqrt{2}\frac{1}{\sqrt{Q_P/2}}c_1\left(\frac{E_{b1}}{N_0}\right)}, \quad (27)$$

$$\mu_{13} = \frac{\sqrt{2}\frac{1}{\sqrt{Q_P/2}}c_1\left(\frac{E_{b1}}{N_0}\right) - \left(R_b - \sqrt{d\left(\frac{E_{b1}}{N_0}\right)}\right)}{\sqrt{2}\frac{1}{\sqrt{Q_P/2}}c_1\left(\frac{E_{b1}}{N_0}\right) + \left(R_b + \sqrt{d\left(\frac{E_{b1}}{N_0}\right)}\right)}, \quad (28)$$

$$\mu_{23} = \frac{\sqrt{2}\frac{1}{\sqrt{Q_P/2}}c_1\left(\frac{E_{b1}}{N_0}\right) + \left(R_b - \sqrt{d\left(\frac{E_{b1}}{N_0}\right)}\right)}{\sqrt{2}\frac{1}{\sqrt{Q_P/2}}c_1\left(\frac{E_{b1}}{N_0}\right) - \left(R_b + \sqrt{d\left(\frac{E_{b1}}{N_0}\right)}\right)}, \quad (29)$$

$$\mu_{43} = \frac{R_b}{\sqrt{d\left(\frac{E_{b1}}{N_0}\right)}}. \quad (30)$$

In the above equations, we have $d\left(\frac{E_{b1}}{N_0}\right) = R_b^2 + 2R_b\left(1+\frac{1}{Q_P/2}\right)c_1\left(\frac{E_{b1}}{N_0}\right) + 2\frac{1}{Q_P/2}\left[c_1\left(\frac{E_{b1}}{N_0}\right)\right]^2$, where $c_1\left(\frac{E_{b1}}{N_0}\right) = (K-1) + \frac{R_1}{E_{b1}/N_0}$.

4) Asymptotic Analysis—Perfect CSI: While the complexity of the above expressions makes it difficult to gain an intuitive understanding of the probability of error, the usefulness of this closed-form result becomes apparent when we consider the asymptotic case of perfect CSI. Suppose we have a completely static channel, such that the fade amplitudes are constant over an infinitely long data frame (i.e., $Q \to \infty$). If we let $Q_P \to \infty$, then the error terms in (24) vanish, and the channel estimation becomes perfect. Since $\lim_{Q_P\to\infty} d\left(\frac{E_{b1}}{N_0}\right) = R_b\left(R_b + 2c_1\left(\frac{E_{b1}}{N_0}\right)\right)$, we have $\lim_{Q_P\to\infty}\mu_{31} = \lim_{Q_P\to\infty}\mu_{41} = 1$, $\lim_{Q_P\to\infty}\mu_{13} = \lim_{Q_P\to\infty}\mu_{23} = -1$, and $\lim_{Q_P\to\infty}\mu_{43} = \sqrt{\frac{R_b}{R_b+2c_1\left(\frac{E_{b1}}{N_0}\right)}} = \sqrt{\frac{\bar{\gamma}_P}{1+\bar{\gamma}_P}}$, where $\bar{\gamma}_P = \frac{R_b}{2c_1\left(\frac{E_{b1}}{N_0}\right)} = \frac{1}{2}\left(\frac{1}{MR_1/N}\frac{E_{b1}}{N_0}\right)\frac{1}{1+(K-1)\frac{1}{R_1}\frac{E_{b1}}{N_0}}$. Using these results, we finally obtain

$$\lim_{Q_P\to\infty} P_e = \left(\frac{1-\mu}{2}\right)^a \sum_{i=0}^{a-1}\binom{a-1+i}{i}\left(\frac{1+\mu}{2}\right)^i, \quad (31)$$

where $\mu = \sqrt{\frac{\bar{\gamma}_P}{1+\bar{\gamma}_P}}$. Note that (31) is simply the probability of error of an ideal maximal ratio combiner with $4MR_1/N$-th order diversity and an average signal-to-interference-plus-noise ratio (SINR) per diversity branch of $\bar{\gamma}_P$ [24, Eqs. (14.4-15)–(14.4-16)].

B. MC-DS-CDMA

1) Demodulator Output: The demodulator output at frequency $f_{m,i}$ of the v-th antenna during the q-th time slot is given by

$$W_{q,v,m,i} = A_{2e}\sqrt{N}g^{(1)}_{v,u,m,i} + I_{W_{q,v,m,i}} + N_{W_{q,v,m,i}}, \quad q = 1,\ldots,Q_P, \quad (32)$$

$$Y_{q,v,m,i} = A_{2d}\sqrt{N}\sum_{u=1}^{2} b^{(1)}_{p,q,u,m}\, g^{(1)}_{v,u,m,i} + I_{Y_{q,v,m,i}} + N_{Y_{q,v,m,i}}, \quad q = Q_P+1,\ldots,Q, \quad (33)$$

where

$$I_{W_{q,v,m,i}} = \frac{1}{\sqrt{N}}\sum_{n=1}^{N} C^{(1)}_{p,q,n}\sum_{k=2}^{K}\sum_{u=1}^{2} g^{(k)}_{v,u,m,i}\sum_{p'=-\infty}^{\infty}\sum_{q'=1}^{Q} \cdot \sum_{n'=1}^{N} A_{2,q'} b^{(k)}_{p',q',u,m} C^{(k)}_{p',q',n'} \cdot x_2\{t-[(p'Q+q'-1)N+n'-1]T_c - \tau^{(k)}\}\big|_{t=[(pQ+q-1)N+n-1]T_c} \quad (34)$$

and

$$N_{W_{q,v,m,i}} = \frac{1}{\sqrt{N}}\sum_{n=1}^{N} C^{(1)}_{p,q,n} \cdot \left(\tilde{n}_v(t) * \tilde{h}_{m,i,2}(t)\right)\Big|_{t=[(pQ+q-1)N+n-1]T_c} \quad (35)$$

correspond to the MAI and AWGN terms, respectively. Again, the expressions for $I_{Y_{q,v,m,i}}$ and $N_{Y_{q,v,m,i}}$ are identical to (34) and (35), respectively. As in the MC-CDMA analysis, $W_{q,v,m,i}$ and $Y_{q,v,m,i}$ are both zero-mean complex Gaussian random variables in the single-user case and are approximated as zero-mean complex Gaussian random variables when K is large.

2) Channel Estimation: The expression for $\hat{W}_{v,u,m,i}$ is obtained by substituting (32) into (3). For MC-DS-CDMA, we require a normalizing constant of $A_0 = A_{2e}\sqrt{N}$.

3) Probability of Error: From Appendix C, the probability of error is derived as

$$P_e = \left(\frac{1-\mu}{2}\right)^{4R_2}\sum_{i=0}^{4R_2-1}\binom{4R_2-1+i}{i}\left(\frac{1+\mu}{2}\right)^i, \quad (36)$$

where

$$\mu = \sqrt{\frac{\bar{\gamma}}{1+\bar{\gamma}}}, \quad (37)$$

$$\bar{\gamma} = \frac{1}{2}\left\{\left(1+\frac{1}{Q_P/2}\right)c_2\left(\frac{E_{b2}}{N_0}\right) + \frac{1}{Q_P/2}\left[c_2\left(\frac{E_{b2}}{N_0}\right)\right]^2\right\}^{-1}, \quad (38)$$

and $c_2\left(\frac{E_{b2}}{N_0}\right) = \frac{K-1}{N} + \frac{R_2}{E_{b2}/N_0}$. Note that this is just the probability of error of an ideal maximal ratio combiner with $4R_2$-th order diversity, except that the average SINR per diversity branch has been replaced by $\bar{\gamma}$ of (38) [24, Eqs. (14.4-15),(14.4-16)].

4) Asymptotic Analysis—Perfect CSI: Once again, the results for perfect CSI can be obtained by assuming both a static channel and an infinitely long data frame ($Q \to \infty$) and then computing the limits of the expressions in (36)–(38) as $Q_P \to \infty$. Since Q_P is only present in $\bar{\gamma}$, we can simply replace $\bar{\gamma}$ in μ with $\bar{\gamma}_P \triangleq \lim_{Q_P\to\infty}\bar{\gamma} = \frac{1}{2c_2\left(\frac{E_{b2}}{N_0}\right)} = \frac{1}{2}\left(\frac{1}{R_2}\frac{E_{b2}}{N_0}\right)\frac{1}{1+\frac{K-1}{N}\frac{1}{R_2}\frac{E_{b2}}{N_0}}$.

V. Numerical Results

A. Review of General Trends

We briefly summarize the general trends observed in Scenario #2 of [20] for the SISO system. When $M > 1$ and $K = 1$, the error probability curves for MC-CDMA and MC-DS-CDMA always cross. This cross-over point, which we denote by $(\Delta, P_{e,\Delta})$, implies that $P_{e,\text{MC-DS-CDMA}} < P_{e,\text{MC-CDMA}}$ for $E_b/N_0 < \Delta$ and $P_{e,\text{MC-DS-CDMA}} > P_{e,\text{MC-CDMA}}$ for $E_b/N_0 > \Delta$. Likewise, we also have $(E_b/N_0)_{\text{MC-DS-CDMA}} < (E_b/N_0)_{\text{MC-CDMA}}$ for $P_e > P_{e,\Delta}$ and $(E_b/N_0)_{\text{MC-DS-CDMA}} > (E_b/N_0)_{\text{MC-CDMA}}$ for $P_e < P_{e,\Delta}$. When $M > 1$ and $K > 1$, the MC-DS-CDMA and MC-CDMA curves cross only if Q_P is sufficiently large; otherwise, MC-DS-CDMA gives a lower P_e for all E_b/N_0. This is due to the fact that our detection schemes only involve matched filtering and lack a mechanism for combatting MAI. As a result, an error floor is present at high E_b/N_0, and the curves for both multi-carrier schemes flatten out.

In the figures to be presented shortly, we will see that these trends for the SISO system also apply to our MIMO system. This is because the multi-carrier comparisons in both cases are centered around the trade-off between diversity gain and channel estimation errors.

B. SISO vs. MIMO Comparison

Using the closed-form expressions for the bit error probabilities of MC-CDMA and MC-DS-CDMA presented in the previous section and in Section III-E of [20], we compare the MIMO results with those of Scenario #2 of the SISO system to study the impact of the additional diversity on the multi-carrier comparison. For both the SISO and MIMO systems, we assume $S_1 = MR_1 = 512$ and $S_2 = MR_2 = 8$ sub-carriers for MC-CDMA and MC-DS-CDMA, respectively, where the processing gain of each MC-DS-CDMA sub-band is $N = 64$. We set $E_{b1} = E_{b2} = E_b$ and consider both $K = 1$ and $K = 16$. The overall diversity gains per data symbol in MC-DS-CDMA and MC-CDMA are equal to R_2 and MR_1/N, respectively, in the SISO system, and $4R_2$ and $4MR_1/N$, respectively, in the MIMO system. As we pointed out earlier in Section III, MC-CDMA has M times the diversity of MC-DS-CDMA. Thus, when $M = 1$, both multi-carrier schemes have equal diversity, and the probability of error was shown to be always lower in MC-DS-CDMA due to more reliable channel estimation [20]. Henceforth, we only consider $M > 1$. Since the transmission of pilot symbols during the estimation phase occurs during every time slot in the SISO system, but only during every other time slot at each antenna in the MIMO system, we assume $Q_P = 16$ for the SISO system and consider both $Q_P = 16$ and $Q_P = 32$ for the MIMO system. When $Q_P = 16$, the MIMO system maintains the same throughput as the SISO system[6] (i.e., both systems transmit Q_D data symbols per frame at each sub-carrier), but when $Q_P = 32$, the MIMO system uses the same amount of total energy (i.e., same number of pilot symbols) as the SISO system to estimate each channel gain.

[6]We assume the SISO and MIMO systems use data frames of the same length (i.e., same Q).

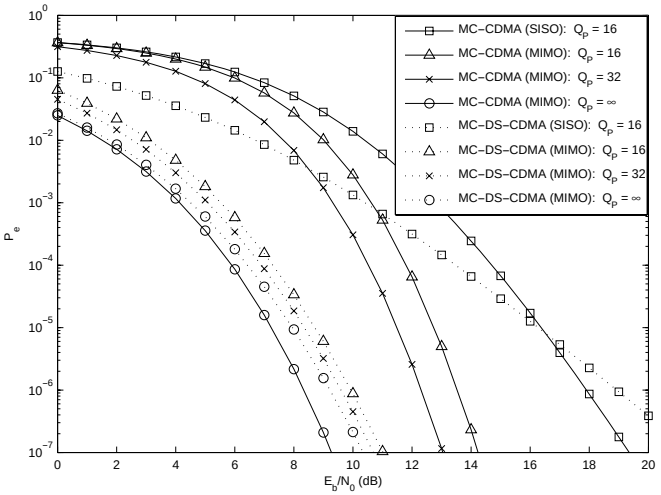

Fig. 6. SISO vs. MIMO: $K = 1$, $M = 2$, $R_2 = 4$, $MR_1/N = 8$. The orders of diversity (per data symbol) in MC-DS-CDMA and MC-CDMA are equal to 4 and 8, respectively, in the SISO system, and 16 and 32, respectively, in the MIMO system.

First, we consider the single-user scenario and compare the SISO and MIMO results against a target bit error rate of $P_e^* = 10^{-5}$. The case $M = 2$ is examined in Fig. 6. Here, MC-CDMA has twice the frequency diversity of MC-DS-CDMA. Note that the MC-DS-CDMA and MC-CDMA curves for the SISO system cross near P_e^*, which means that both multi-carrier schemes require approximately the same E_b/N_0 to achieve P_e^*. For the MIMO system, however, we observe that for both $Q_P = 16$ and $Q_P = 32$, the E_b/N_0 values required to achieve P_e^* are lower in MC-DS-CDMA by at least 3dB. Even if we reduce the target bit error rate to $P_e^* = 10^{-7}$, the required E_b/N_0 values are still lower in MC-DS-CDMA. Next, we consider $M = 8$. We observe in Fig. 7 that the cross-over points in the SISO case and in both instances of the MIMO case occur at P_e values which are greater than $P_e^* = 10^{-5}$. Thus, MC-CDMA achieves P_e^* at lower E_b/N_0 values than MC-DS-CDMA in both the SISO and MIMO cases, although the differences in the required E_b/N_0 values are much smaller in the two MIMO cases. Based on these results for $M = 2$ and $M = 8$, we conclude that for $K = 1$, the performance gains obtained by MC-DS-CDMA from the addition of spatial diversity are enough to offset the difference in frequency diversity between the two schemes when M is small, but not when M is large.

Now, consider a multi-user scenario with $K = 16$. When $M = 2$, we see in Fig. 8 that the MC-CDMA and MC-DS-CDMA curves do not cross in either the SISO or MIMO cases. Furthermore, at a given E_b/N_0, the differences in probability of error between the two schemes are much larger in the two MIMO cases than in the SISO case. This implies that in order for the MC-CDMA and MC-DS-CDMA curves to cross, we will have to use a larger Q_P in the MIMO case than in the SISO case. When $M = 8$, the curves for the two schemes in Fig. 9 do cross in the case of the SISO system when $Q_P = 16$. In the MIMO system, however, a cross-over point does not exist for either $Q_P = 16$ or $Q_P = 32$; we must use $Q_P > 32$ in order for the curves to cross. Thus, we conclude that the additional diversity increases the value of Q_P required for the

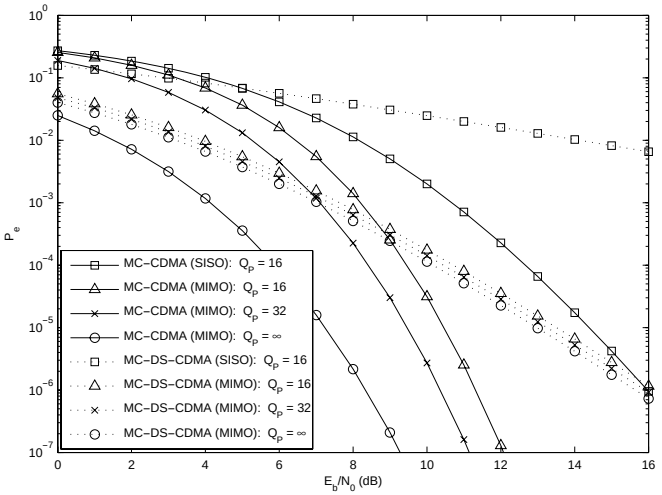

Fig. 7. SISO vs. MIMO: $K = 1$, $M = 8$, $R_2 = 1$, $MR_1/N = 8$. The orders of diversity (per data symbol) in MC-DS-CDMA and MC-CDMA are equal to 1 and 8, respectively, in the SISO system, and 4 and 32, respectively, in the MIMO system.

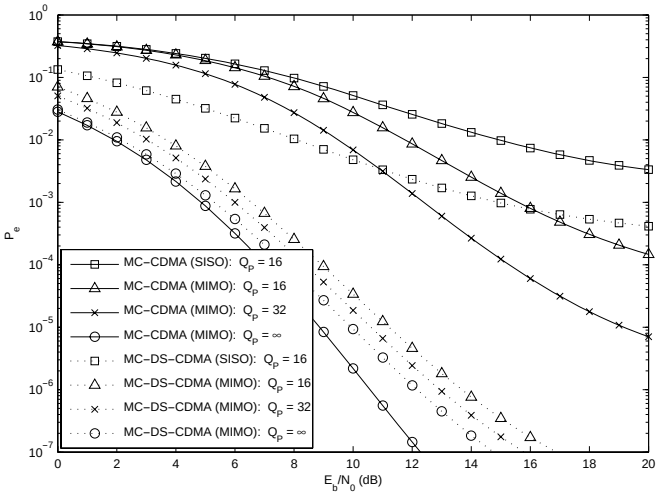

Fig. 8. SISO vs. MIMO: $K = 16$, $M = 2$, $R_2 = 4$, $MR_1/N = 8$.

MC-CDMA and MC-DS-CDMA curves to cross and for there to be a trade-off in performance between the two multi-carrier schemes.

VI. Conclusion

Our previous comparison between MC-DS-CDMA and MC-CDMA focused on the trade-off between diversity gain and channel estimation errors, but only a SISO system was considered. In this work, we incorporated spatial diversity into the comparison by using a MIMO system employing Alamouti space-time block coding. To quantify the effects of this additional diversity, we derived closed-form expressions for the bit error probabilities of the two multi-carrier schemes, and we compared the results of the MIMO system against those of the SISO system. Since we only considered those cases where MC-CDMA has higher frequency diversity than MC-DS-CDMA, we argued that the additional diversity benefits MC-DS-CDMA more than MC-CDMA. It was shown for the case of a single user that these gains for MC-DS-CDMA can offset the difference in frequency diversity between the two schemes when M is small, but not when M is large, where M represents the number of parallel data streams. Also, when matched-filter-based detection is used for the case of multiple users, our results showed that the additional diversity increases the number of pilot symbols required to force a performance trade-off between the two schemes (i.e., to get the MC-CDMA and MC-DS-CDMA curves to cross).

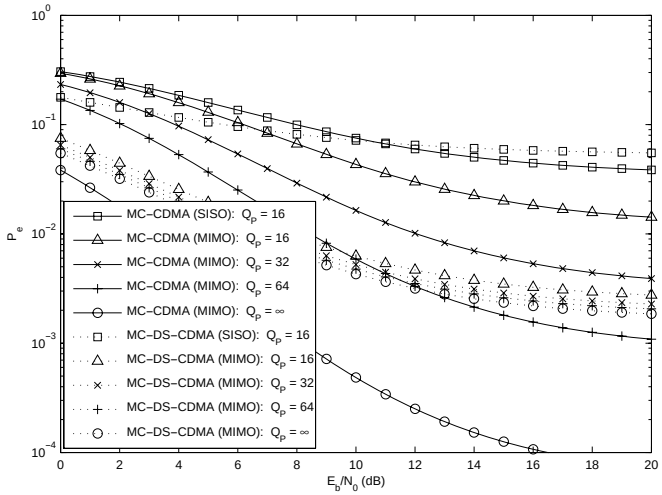

Fig. 9. SISO vs. MIMO: $K = 16$, $M = 8$, $R_2 = 1$, $MR_1/N = 8$.

Appendix A
Hermitian Quadratic Forms in Complex Gaussian Random Variables

Consider the general Hermitian quadratic form

$$Z = \mathbf{v}^H \mathbf{F} \mathbf{v}, \tag{39}$$

where $\mathbf{v} = [v_1 \cdots v_N]^T$ is a column vector of N jointly distributed *zero-mean* complex Gaussian random variables, and $\mathbf{F}$ is an $N \times N$ Hermitian matrix. Define the $N \times N$ covariance matrix of $\mathbf{v}$ as

$$\mathbf{R} = \frac{1}{2} E\left[\mathbf{v}\mathbf{v}^H\right]. \tag{40}$$

The characteristic function of Z, $\Phi_Z(j\upsilon) \triangleq E[e^{j\upsilon Z}]$, is given by [25, Eq. (B-3-16)]

$$\Phi_Z(j\upsilon) = \frac{1}{\det\left(\mathbf{I}_N - 2j\upsilon\mathbf{R}\mathbf{F}\right)} = \prod_{n=1}^{\Lambda} \left(1 - 2j\upsilon\lambda_n\right)^{-m_n} = \sum_{n=1}^{\Lambda} \sum_{k=1}^{m_n} \frac{c_{n,(m_n-k+1)}}{\left(1 - 2j\upsilon\lambda_n\right)^k}, \tag{41}$$

where $\lambda_1, \ldots, \lambda_\Lambda$ are the $\Lambda \leq N - m_0$ *distinct non-zero eigenvalues* of the matrix $\mathbf{RF}$ with multiplicities $m_1, \ldots, m_\Lambda$ such that $\sum_{i=1}^{\Lambda} m_i = N - m_0$, and m_0 is the number of eigenvalues of $\mathbf{RF}$ equal to zero.[7] The last equality in (41) is obtained by applying a partial fraction expansion (PFE). The

[7]The eigenvalues equal to zero only contribute a factor of 1 to $\Phi_Z(j\upsilon)$.

PFE coefficient $c_{n,k}$ can be written in closed-form as [26]

$$c_{n,k} = \prod_{\substack{r=1 \\ r\neq n}}^{\Lambda} \left(1-\frac{\lambda_r}{\lambda_n}\right)^{-m_r} \sum_{\Omega_n} \cdot \prod_{\substack{p=1 \\ p\neq n}}^{\Lambda} \binom{m_p-1+i_p}{i_p} \left(1-\frac{\lambda_n}{\lambda_p}\right)^{-i_p}, \quad (42)$$

where Ω_n denotes the set of integers $\{i_1,\ldots,i_{n-1},i_{n+1},\ldots,i_\Lambda\}$ such that $\sum_{p=1,p\neq n}^{\Lambda} i_p = k-1$. By defining

$$\mu_{mn} = \frac{\lambda_m+\lambda_n}{\lambda_m-\lambda_n}, \quad m\neq n, \quad (43)$$

we have $\left(1-\frac{\lambda_m}{\lambda_n}\right)^{-1} = \frac{1-\mu_{mn}}{2}$ and $\left(1-\frac{\lambda_n}{\lambda_m}\right)^{-1} = \frac{1+\mu_{mn}}{2}$, and we can re-write $c_{n,k}$ as

$$c_{n,k} = \prod_{\substack{r=1 \\ r\neq n}}^{\Lambda} \left(\frac{1-\mu_{rn}}{2}\right)^{m_r} \sum_{\Omega_n} \cdot \prod_{\substack{p=1 \\ p\neq n}}^{\Lambda} \binom{m_p-1+i_p}{i_p} \left(\frac{1+\mu_{pn}}{2}\right)^{i_p}. \quad (44)$$

Assuming binary signaling, the probability of error is derived as [27, Eqs. (46)–(48)]

$$P_e = P[Z<0] = \int_{-\infty}^{0} \frac{1}{2\pi} \int_{-\infty}^{\infty} \Phi_Z(j\upsilon) e^{-j\upsilon x}\, d\upsilon\, dx = \sum_{\substack{n=1 \\ \lambda_n<0}}^{\Lambda} \sum_{k=1}^{m_n} c_{n,k}. \quad (45)$$

In general, both the eigenvalues of $\mathbf{RF}$ and the $\{c_{n,k}\}$ will need to be evaluated numerically. But if Λ is small, then (44) may reduce to a manageable closed-form expression, and it may also be possible to derive the eigenvalues of $\mathbf{RF}$ in closed form. For example, when $\Lambda = 2$, the probability of error reduces to [24, Eq. (14.4-15)].

Appendix B
Derivation of Probability of Error: MC-CDMA

We derive the probability of error for MC-CDMA using the approach given in Appendix A. We assume a $+1$ is transmitted (i.e., $a^{(1)}_{p,q,m} = +1$), and we condition on $a^{(1)}_{p,q+1,m}$. From (40) and (13), the covariance matrix of $\mathbf{v}_{q,m}$ is equal to

$$\mathbf{R} = \frac{1}{2}E[\mathbf{v}_{q,m}\mathbf{v}^H_{q,m}] = \begin{bmatrix} \mathbf{\Sigma}_{ww} & \mathbf{\Sigma}_{wy} \\ \mathbf{\Sigma}^H_{wy} & \mathbf{\Sigma}_{yy} \end{bmatrix}, \quad (46)$$

where

$$\mathbf{\Sigma}_{ww} \triangleq \frac{1}{2}E[\mathbf{w}_m\mathbf{w}^H_m], \quad (47)$$

$$\mathbf{\Sigma}_{yy} \triangleq \frac{1}{2}E[\mathbf{y}_{q,m}\mathbf{y}^H_{q,m}], \quad (48)$$

$$\mathbf{\Sigma}_{wy} \triangleq \frac{1}{2}E[\mathbf{w}_m\mathbf{y}^H_{q,m}]. \quad (49)$$

As a result, we have the partitioned matrix

$$\mathbf{RF} = \frac{1}{2}\begin{bmatrix} \mathbf{\Sigma}_{wy} & \mathbf{\Sigma}_{ww} \\ \mathbf{\Sigma}_{yy} & \mathbf{\Sigma}^H_{wy} \end{bmatrix}, \quad (50)$$

and its characteristic polynomial can be expanded as [23, Sec. A1.1.3]

$$\begin{aligned} &\det(\lambda\mathbf{I}_{8R_1} - \mathbf{RF}) \\ &= \begin{vmatrix} \lambda\mathbf{I}_{4R_1} - \frac{1}{2}\mathbf{\Sigma}_{wy} & -\frac{1}{2}\mathbf{\Sigma}_{ww} \\ -\frac{1}{2}\mathbf{\Sigma}_{yy} & \lambda\mathbf{I}_{4R_1} - \frac{1}{2}\mathbf{\Sigma}^H_{wy} \end{vmatrix} \\ &= \det\left(\lambda\mathbf{I}_{4R_1} - \frac{1}{2}\mathbf{\Sigma}_{wy}\right) \cdot \det\left\{\left(\lambda\mathbf{I}_{4R_1} - \frac{1}{2}\mathbf{\Sigma}^H_{wy}\right) - \frac{1}{4}\mathbf{\Sigma}_{yy}\left(\lambda\mathbf{I}_{4R_1} - \frac{1}{2}\mathbf{\Sigma}_{wy}\right)^{-1}\mathbf{\Sigma}_{ww}\right\}. \end{aligned} \quad (51)$$

We show in [22, Appendix M] that the matrices $\mathbf{\Sigma}_{ww}$, $\mathbf{\Sigma}_{yy}$, and $\mathbf{\Sigma}_{wy}$ are derived as

$$\mathbf{\Sigma}_{ww} = \mathbf{I}_{MR_1/N} \otimes \frac{1}{2}\left[\mathbf{A}_{R_b} + \frac{1}{Q_P/2}\, c_1\left(\frac{E_{b1}}{N_0}\right)\mathbf{I}_{R_b}\right] \otimes \mathbf{I}_4, \quad (52)$$

$$\mathbf{\Sigma}_{yy} = \mathbf{I}_{MR_1/N} \otimes \frac{E_{b1}}{R_1}\left[\mathbf{A}_{R_b} + c_1\left(\frac{E_{b1}}{N_0}\right)\mathbf{I}_{R_b}\right] \otimes \mathbf{I}_4, \quad (53)$$

$$\mathbf{\Sigma}_{wy} = \mathbf{I}_{MR_1/N} \otimes \frac{1}{2}\sqrt{\frac{E_{b1}}{R_1}}\left[\mathbf{A}_{R_b} \otimes \mathbf{B}_2\left(a^{(1)}_{p,q+1,m}\right) \otimes \mathbf{I}_2\right], \quad (54)$$

where $\mathbf{A}_{R_b}$ is the $R_b \times R_b$ all-ones matrix, $c_1\left(\frac{E_{b1}}{N_0}\right) \triangleq (K-1) + \frac{R_1}{E_{b1}/N_0}$, and

$$\mathbf{B}_2(\epsilon) \triangleq \begin{bmatrix} 1 & -\epsilon \\ \epsilon^* & 1 \end{bmatrix}. \quad (55)$$

Substituting these expressions into (51), we can show after much algebraic manipulation that the characteristic polynomial of $\mathbf{RF}$ reduces to [22, Appendix M]

$$\det(\lambda\mathbf{I}_{8R_1} - \mathbf{RF}) = [W(\lambda)]^{4(R_1-MR_1/N)} \cdot [T(\lambda)]^{2MR_1/N}, \quad (56)$$

where

$$W(\lambda) = \lambda^2 - \frac{E_{b1}}{8R_1}\frac{1}{Q_P/2}\left[c_1\left(\frac{E_{b1}}{N_0}\right)\right]^2, \quad (57)$$

$$T(\lambda) = \lambda^4 + b\lambda^3 + c\lambda^2 + d\lambda + e, \quad (58)$$

$$b = -\sqrt{\frac{E_{b1}}{R_1}}R_b, \quad (59)$$

$$c = \frac{E_{b1}}{4R_1}\left\{R_b^2 - R_b\left(1+\frac{1}{Q_P/2}\right)c_1\left(\frac{E_{b1}}{N_0}\right) - \frac{1}{Q_P/2}\left[c_1\left(\frac{E_{b1}}{N_0}\right)\right]^2\right\}, \quad (60)$$

$$d = \sqrt{\frac{E_{b1}}{R_1}}\frac{E_{b1}}{8R_1}R_b\, c_1\left(\frac{E_{b1}}{N_0}\right) \cdot \left[R_b\left(1+\frac{1}{Q_P/2}\right) + \frac{1}{Q_P/2}c_1\left(\frac{E_{b1}}{N_0}\right)\right], \quad (61)$$

$$e = \left(\frac{E_{b1}}{8R_1}\right)^2\left[c_1\left(\frac{E_{b1}}{N_0}\right)\right]^2 \cdot \left[R_b\left(1+\frac{1}{Q_P/2}\right) + \frac{1}{Q_P/2}c_1\left(\frac{E_{b1}}{N_0}\right)\right]^2. \quad (62)$$

Since the eigenvalues of $\mathbf{RF}$ are given by the solutions of $\det(\lambda \mathbf{I}_{8R_1} - \mathbf{RF}) = 0$, we first solve for the roots of $[W(\lambda)]^{4(R_1 - MR_1/N)}$, along with their corresponding multiplicities, to obtain

$$\lambda_1 = -\frac{1}{2}\sqrt{\frac{E_{b1}}{2R_1}}\frac{1}{\sqrt{Q_P/2}}\, c_1\left(\frac{E_{b1}}{N_0}\right), \tag{63}$$

$$\lambda_2 = \frac{1}{2}\sqrt{\frac{E_{b1}}{2R_1}}\frac{1}{\sqrt{Q_P/2}}\, c_1\left(\frac{E_{b1}}{N_0}\right), \tag{64}$$

and

$$m_1 = 4(R_1 - MR_1/N), \tag{65}$$

$$m_2 = 4(R_1 - MR_1/N). \tag{66}$$

Likewise, using the general method for solving quartic polynomials [28, Sec. 2.3], the solutions to $[T(\lambda)]^{2MR_1/N} = 0$ are given by

$$\lambda_3 = \frac{1}{4}\sqrt{\frac{E_{b1}}{R_1}}\left(R_b - \sqrt{d\left(\frac{E_{b1}}{N_0}\right)}\right), \tag{67}$$

$$\lambda_4 = \frac{1}{4}\sqrt{\frac{E_{b1}}{R_1}}\left(R_b + \sqrt{d\left(\frac{E_{b1}}{N_0}\right)}\right), \tag{68}$$

and

$$m_3 = 4MR_1/N, \tag{69}$$

$$m_4 = 4MR_1/N, \tag{70}$$

where $d\left(\frac{E_{b1}}{N_0}\right) \triangleq R_b^2 + 2R_b\left(1 + \frac{1}{Q_P/2}\right)c_1\left(\frac{E_{b1}}{N_0}\right) + 2\frac{1}{Q_P/2}\left[c_1\left(\frac{E_{b1}}{N_0}\right)\right]^2$. Thus, $\mathbf{RF}$ has $\Lambda = 4$ distinct eigenvalues. For $\frac{E_{b1}}{N_0} > 0$, we have $c_1\left(\frac{E_{b1}}{N_0}\right) > 0$, which implies $d\left(\frac{E_{b1}}{N_0}\right) > R_b^2$. λ_1 and λ_3 are then the only negative eigenvalues, and the expression for the probability of error in (45) reduces to

$$P_e = \sum_{k=1}^{4(R_1 - MR_1/N)} c_{1,k} + \sum_{k=1}^{4MR_1/N} c_{3,k}. \tag{71}$$

By substituting (44) into (71), we can show after a series of manipulations that P_e is equal to (25) [22, Appendix M]. The expressions for μ_{21}, μ_{31}, μ_{41}, μ_{13}, μ_{23}, and μ_{43} are obtained by using (63)–(64) and (67)–(68) in (43), and we can easily verify that $\mu_{21} = 0$.

APPENDIX C
DERIVATION OF PROBABILITY OF ERROR: MC-DS-CDMA

The probability of error for MC-DS-CDMA is also derived using the approach presented in Appendix A. Again, we assume $a^{(1)}_{p,q,m} = +1$, and we condition on $a^{(1)}_{p,q+1,m}$. The expressions for $\mathbf{R}$, $\mathbf{\Sigma}_{ww}$, $\mathbf{\Sigma}_{yy}$, $\mathbf{\Sigma}_{wy}$, and $\mathbf{RF}$ in (46)–(50) still hold. For MC-DS-CDMA, the matrices $\mathbf{\Sigma}_{ww}$, $\mathbf{\Sigma}_{yy}$, and $\mathbf{\Sigma}_{wy}$ are derived as [22, Appendix L]

$$\mathbf{\Sigma}_{ww} = \frac{1}{2}\left[1 + \frac{1}{Q_P/2}\, c_2\left(\frac{E_{b2}}{N_0}\right)\right]\mathbf{I}_{4R_2}, \tag{72}$$

$$\mathbf{\Sigma}_{yy} = \frac{E_{b2}}{R_2}\left[1 + c_2\left(\frac{E_{b2}}{N_0}\right)\right]\mathbf{I}_{4R_2}, \tag{73}$$

$$\mathbf{\Sigma}_{wy} = \frac{1}{2}\sqrt{\frac{E_{b2}}{R_2}}\left[\mathbf{I}_{R_2} \otimes \mathbf{B}_2\left(a^{(1)}_{p,q+1,m}\right) \otimes \mathbf{I}_2\right], \tag{74}$$

where $c_2\left(\frac{E_{b2}}{N_0}\right) \triangleq \frac{K-1}{N} + \frac{R_2}{E_{b2}/N_0}$ and $\mathbf{B}_2(\epsilon)$ is defined in (55). Substituting these expressions into (51) and replacing R_1 with R_2, we can show that the characteristic polynomial of $\mathbf{RF}$ reduces to [22, Appendix L]

$$\det(\lambda \mathbf{I}_{8R_2} - \mathbf{RF}) = \left(\lambda^2 - b\lambda - c\right)^{4R_2}, \tag{75}$$

where

$$b = \frac{1}{2}\sqrt{\frac{E_{b2}}{R_2}}, \tag{76}$$

$$c = \frac{E_{b2}}{8R_2}\left\{\left(1 + \frac{1}{Q_P/2}\right)c_2\left(\frac{E_{b2}}{N_0}\right) + \frac{1}{Q_P/2}\left[c_2\left(\frac{E_{b2}}{N_0}\right)\right]^2\right\}. \tag{77}$$

The equation $\det(\lambda \mathbf{I}_{8R_2} - \mathbf{RF}) = 0$ yields $\Lambda = 2$ distinct eigenvalues, both of multiplicity $m_1 = m_2 = 4R_2$:

$$\lambda_1 = \frac{b - \sqrt{b^2 + 4c}}{2}, \quad \lambda_2 = \frac{b + \sqrt{b^2 + 4c}}{2}. \tag{78}$$

For $\frac{E_{b2}}{N_0} > 0$, we have $c_2\left(\frac{E_{b2}}{N_0}\right) > 0$, which implies $b^2 + 4c > b^2$. Substituting (44) into (45) and using the fact that λ_1 is the only negative eigenvalue, we can finally show that

$$P_e = \sum_{k=1}^{4R_2} c_{1,k} = \left(\frac{1 - \mu_{21}}{2}\right)^{4R_2} \sum_{i=0}^{4R_2 - 1}\binom{4R_2 - 1 + i}{i} \cdot \left(\frac{1 + \mu_{21}}{2}\right)^i, \tag{79}$$

where $\mu_{21} = \frac{\lambda_2 + \lambda_1}{\lambda_2 - \lambda_1} = \frac{b}{\sqrt{b^2 + 4c}} = \sqrt{\frac{\bar{\gamma}}{1 + \bar{\gamma}}}$, and $\bar{\gamma} = \frac{b^2}{4c}$ can be shown to reduce to the expression in (38).

REFERENCES

[1] E. A. Sourour and M. Nakagawa, "Performance of orthogonal multicarrier CDMA in a multipath fading channel," *IEEE Trans. Commun.*, vol. 44, no. 3, pp. 356–367, Mar. 1996.

[2] S. Kondo and L. B. Milstein, "Performance of multicarrier DS CDMA systems," *IEEE Trans. Commun.*, vol. 44, no. 2, pp. 238–246, Feb. 1996.

[3] D. Lee and L. B. Milstein, "Comparison of multicarrier DS-CDMA broadcast systems in a multipath fading channel," *IEEE Trans. Commun.*, vol. 47, no. 12, pp. 1897–1904, Dec. 1999.

[4] W. Xu and L. B. Milstein, "On the performance of multicarrier RAKE systems," *IEEE Trans. Commun.*, vol. 49, no. 10, pp. 1812–1823, Oct. 2001.

[5] L. L. Chong and L. B. Milstein, "Error rate of a multicarrier CDMA system with imperfect channel estimates," in *Proc. IEEE Int. Conf. Commun. (ICC'00)*, June 2000, vol. 2, pp. 934–938.

[6] L.-L. Yang and L. Hanzo, "Performance of generalized multicarrier DS-CDMA over Nakagami-m fading channels," *IEEE Trans. Commun.*, vol. 50, no. 6, pp. 956–966, June 2002.

[7] M. Guenach and L. Vandendorpe, "Downlink performance analysis of a BPSK-based WCDMA using conventional RAKE receivers with channel estimation," *IEEE J. Select. Areas Commun.*, vol. 19, no. 11, pp. 2165–2176, Nov. 2001.

[8] N. Yee, J. M. G. Linnartz, and G. Fettweis, "Multicarrier CDMA in indoor wireless radio networks," *IEICE Trans. Commun.*, vol. E77-B, no. 7, pp. 900–904, July 1994.

[9] X. Gui and T. S. Ng, "Performance of asynchronous orthogonal multicarrier CDMA system in frequency selective fading channel," *IEEE Trans. Commun.*, vol. 47, no. 7, pp. 1084–1091, July 1999.

[10] Z. Hou and V. K. Dubey, "Bit error probability of MC-CDMA system over Rayleigh fading channels," in *Proc. IEEE 8th Int. Symp. Spread Spectrum Techniques Appl. (ISSSTA'04)*, Aug. 2004, pp. 320–324.

[11] Z. Kang and K. Yao, "Performance comparison of MC-CDMA over frequency-selective Nakagami-4m and Rayleigh fading channels," in *Proc. IEEE 60th Veh. Technol. Conf. (VTC'04–Fall)*, Sept. 2004, vol. 6, pp. 4228–4232.

[12] Q. Shi and M. Latva-Aho, "Accurate bit-error rate evaluation for synchronous MC-CDMA over Nakagami-m fading channels using moment generating functions," *IEEE Trans. Wireless Commun.*, vol. 4, no. 2, pp. 422–433, Mar. 2005.

[13] R. Prasad and S. Hara, "An overview of multicarrier CDMA," in *Proc. IEEE 4th Int. Symp. Spread Spectrum Techniques Appl. (ISSSTA'96)*, Sept. 1996, vol. 1, pp. 107–114.

[14] S. Abeta, H. Atarashi, M. Sawahashi, and F. Adachi, "Coherent multicarrier/DS-CDMA and MC-CDMA for broadband packet wireless access," in *Proc. IEEE 51st Veh. Technol. Conf. (VTC'00–Spring)*, May 2000, vol. 3, pp. 1918–1922.

[15] S. Abeta, H. Atarashi, and M. Sawahashi, "Forward link capacity of coherent DS-CDMA and MC-CDMA broadband packet wireless access in a multi-cell environment," in *Proc. IEEE 52nd Veh. Technol. Conf. (VTC'00–Fall)*, Sep. 2000, vol. 5, pp. 2213–2218.

[16] H. Atarashi, S. Abeta, and M. Sawahashi, "Broadband packet wireless access appropriate for high-speed and high-capacity throughput," in *Proc. IEEE 53rd Veh. Technol. Conf. (VTC'01–Spring)*, May 2001, vol. 1, pp. 566–570.

[17] S. Suwa, H. Atarashi, and M. Sawahashi, "Performance comparison between MC/DS-CDMA and MC-CDMA for reverse link broadband packet wireless access," in *Proc. IEEE 56th Veh. Technol. Conf. (VTC'02–Fall)*, Sept. 2002, vol. 4, pp. 2076–2080.

[18] R. S. El-Khamy, S. E. Shaaban, I. A. Ghaleb, and H. N. Kheirallah, "The enhanced performance of combined multicarrier and CDMA techniques in multipath fading channels," in *Proc. 21st National Radio Science Conference*, Mar. 2004, pp. C34-1—C34-10.

[19] L. Liu, M. Lei, P. Zhang, K. Hamaguchi, and H. Wakana, "Performance of the uplink multicarrier CDMA systems for WPAN indoor applications on MMW band," in *Proc. IEEE 59th Veh. Technol. Conf. (VTC'04–Spring)*, May 2004, vol. 4, pp. 2027–2031.

[20] A. S. Ling and L. B. Milstein, "Trade-off between diversity and channel estimation errors in asynchronous MC-DS-CDMA and MC-CDMA," *IEEE Trans. Commun.*, vol. 56, no. 4, pp. 584–597, Apr. 2008.

[21] S. M. Alamouti, "A simple transmit diversity technique for wireless communications," *IEEE J. Select. Areas Commun.*, vol. 16, no. 10, pp. 1451–1458, Oct. 1998.

[22] A. S. Ling, "Performance analysis of multi-carrier modulation systems," Ph.D. dissertation, University of California, San Diego (UCSD), La Jolla, CA, 2008.

[23] S. M. Kay, *Fundamentals of Statistical Signal Processing, Vol. 1: Estimation Theory*. Upper Saddle River, NJ: Prentice Hall, 1993.

[24] J. G. Proakis, *Digital Communications*, 4th ed. New York: McGraw-Hill, 2001.

[25] M. Schwartz, W. Bennett, and S. Stein, *Communication Systems and Techniques*. New York: McGraw-Hill, 1966.

[26] I.-M. Kim, "Exact BER analysis of OSTBCs in spatially correlated MIMO channels," *IEEE Trans. Commun.*, vol. 54, no. 8, pp. 1365–1373, Aug. 2006.

[27] S. Manohar, V. Tikiya, R. Annavajjala, and A. Chockalingam, "BER-optimal linear parallel interference cancellation for multicarrier DS-CDMA in Rayleigh fading," *IEEE Trans. Commun.*, vol. 55, no. 6, pp. 1253–1265, June 2007.

[28] D. Zwillinger, *CRC Standard Mathematical Tables and Formulae*, 31st ed. Boca Raton: Chapman & Hall/CRC Press, 2003.

Andrew S. Ling (S'99) received the B.S. degree in electrical engineering from the California Institute of Technology (Caltech), Pasadena, CA, in 1999, and the M.S. and Ph.D. degrees in electrical engineering in 2005 and 2008, respectively, from the University of California at San Diego (UCSD), La Jolla, CA. His research interests include digital communication theory, with a special emphasis on the analysis of spread spectrum communication and multiple-antenna systems.

Laurence B. Milstein (S'66-M'68-SM'75-F'85) received the B.E.E. degree from the City College of New York, New York, in 1964, and the M.S. and Ph.D. degrees in electrical engineering from the Polytechnic Institute of Brooklyn, Brooklyn, NY, in 1966 and 1968, respectively.

From 1968 to 1974, he was with the Space and Communication Group, Hughes Aircraft Company, and from 1974 to 1976, he was with the Department of Electrical and Systems Engineering, Rensselaer Polytechnic Institute, Troy, NY. Since 1976, he has been with the Department of Electrical and Computer Engineering, University of California at San Diego (UCSD), La Jolla, CA, where he was a former Department Chairman, and is currently a Professor holding the Ericsson Chair in Wireless Communication Access Techniques. His current research interests include digital communication theory, with special emphasis on spread-spectrum communication systems. He has also been a Consultant to both government and industry in the areas of radar and communications.

Prof. Milstein was an Associate Editor for communications theory for the IEEE TRANSACTIONS ON COMMUNICATIONS, an Associate Editor for book reviews for the IEEE TRANSACTIONS ON INFORMATION THEORY, an Associate Technical Editor for IEEE COMMUNICATIONS MAGAZINE, and the Editor-in-Chief of the IEEE JOURNAL ON SELECTED AREAS IN COMMUNICATIONS. During 1990 and 1991, he was the Vice President for Technical Affairs of the IEEE Communications Society. He has also been a member of the Board of Governors of both the IEEE Communications Society and the IEEE Information Theory Society, and a former Chair of the IEEE Fellows Selection Committee. He is the recipient of the 1998 Military Communications Conference Long-Term Technical Achievement Award, an Academic Senate 1999 UCSD Distinguished Teaching Award, the IEEE Third Millennium Medal in 2000, the 2000 IEEE Communication Society Armstrong Technical Achievement Award, and the 2002 IEEE Military Communications Conference (MILCOM) Fred Ellersick Award.